J|A|C|S ARTICLES

Published on Web 11/15/2010

Influence of Electrolyte Composition on Liquid-Gated Carbon Nanotube and Graphene Transistors

Iddo Heller,[†] Sohail Chatoor, Jaan Männik, Marcel A. G. Zevenbergen, Cees Dekker, and Serge G. Lemay*[,‡]

Kavli Institute of Nanoscience, Delft University of Technology, Lorentzweg 1, 2628 CJ Delft, The Netherlands

Received June 3, 2010; E-mail: s.g.lemay@utwente.nl

Abstract: Field-effect transistors based on single-walled carbon nanotubes (SWNTs) and graphene can function as highly sensitive nanoscale (bio)sensors in solution. Here, we compare experimentally how SWNT and graphene transistors respond to changes in the composition of the aqueous electrolyte in which they are immersed. We show that the conductance of SWNTs and graphene is strongly affected by changes in the ionic strength, the pH, and the type of ions present, in a manner that can be qualitatively different for graphene and SWNT devices. We show that this sensitivity to electrolyte composition results from a combination of different mechanisms including electrostatic gating, Schottky-barrier modifications, and changes in gate capacitance. Interestingly, we find strong evidence that the sensor response to changes in electrolyte composition is affected by a high density of ionizable groups on both the underlying substrate and the carbon surfaces. We present a model based on the (regulated) surface charge associated with these ionizable groups that explains the majority of our data. Our findings have significant implications for interpreting and optimizing sensing experiments with nanocarbon transistors. This is particularly true for complex biological samples such as cell extracts, growth media, or bodily fluids, for which the complete composition of the solution needs to be considered.

Introduction

The search for high-sensitivity, label-free, miniaturized sensors has led to a wide interest in nanoscale electrostatic and electrochemical sensors. Nanowires,[1] single-walled carbon nanotubes (SWNTs),[2,3] and graphene[4] are excellent candidates to function as the active elements in these sensors.[5] Although multiple studies have already demonstrated the outstanding performance of electrostatic nanosensors, important issues concerning detection limits,[6,7] working mechanisms,[3,8] and optimized sensor layout are still under investigation. This illustrates that, on a microscopic level, our understanding of these promising sensors is far from complete.

We have previously studied the nature of the interaction between adsorbed biomolecules and SWNTs.[8] Here, we investigate whether and how the composition of the aqueous electrolyte influences the conductance of SWNT and graphene transistors. We analyze the magnitude of the electrostatic gating effect and changes in p-type and n-type conductance in response to changes in electrolyte composition. We find that changes in the electrolyte salt concentration, the pH, and the type of ions intricately affect the device conductance. Quantitative modeling supports the conclusions that the sensor response is caused by the interplay between surface charge, the corresponding surface potential, and the spatial distribution of ions.

Improving our understanding of the electrostatic interactions of carbon nanosensors with aqueous environments not only allows for the studying of fundamental ionic interactions on a nanoscale, but it also aids in setting up and interpreting biosensing experiments, studying sensor specificity, and optimizing sensor design.

Materials and Methods

CVD-grown SWNTs and single-layer graphene flakes were electrically contacted on oxidized Si wafers by Cr/Au electrodes patterned by means of electron-beam lithography (see the Supporting Information for details on the fabrication process). Figure 1a and d shows sketches, respectively, of a SWNT and a graphene flake in an electrolyte-gated transistor layout.[9] We applied a small bias voltage across source and drain electrodes while monitoring the source-drain current I_{sd} passing through the devices. A home-built flow cell with access for a reference electrode was used to contain the aqueous electrolyte on top of the device. All solutions

[†] Present address: Department of Physics and Astronomy, VU University, De Boelelaan 1081, 1081 HV Amsterdam, The Netherlands.

[‡] Present address: MESA+ Institute and Faculty of Science and Technology, University of Twente, P.O. Box 217, 7500 AE Enschede, The Netherlands.

(1) Patolsky, F.; Timko, B. P.; Zheng, G.; Lieber, C. M. *MRS Bull.* **2007**, *32*, 142–149.
(2) Kauffman, D. R.; Star, A. *Angew. Chem., Int. Ed.* **2008**, *47*, 6550–6570.
(3) Kauffman, D. R.; Star, A. *Chem. Soc. Rev.* **2008**, *37*, 1197–1206.
(4) Schedin, F.; Geim, A. K.; Morozov, S. V.; Hill, E. W.; Blake, P.; Katsnelson, M. I.; Novoselov, K. S. *Nat. Mater.* **2007**, *6*, 652–655.
(5) Yang, W.; Ratinac, K. R.; Ringer, S. P.; Thordarson, P.; Gooding, J. J.; Braet, F. *Angew. Chem., Int. Ed.* **2010**, *49*, 2114–2138.
(6) Sheehan, P. E.; Whitman, L. J. *Nano Lett.* **2005**, *5*, 803–807.
(7) Squires, T. M.; Messinger, R. J.; Manalis, S. R. *Nat. Biotechnol.* **2008**, *26*, 417–426.
(8) Heller, I.; Janssens, A. M.; Männik, J.; Minot, E. D.; Lemay, S. G.; Dekker, C. *Nano Lett.* **2008**, *8*, 591–595.
(9) Rosenblatt, S.; Yaish, Y.; Park, J.; Gore, J.; Sazonova, V.; McEuen, P. L. *Nano Lett.* **2002**, *2*, 869–872.

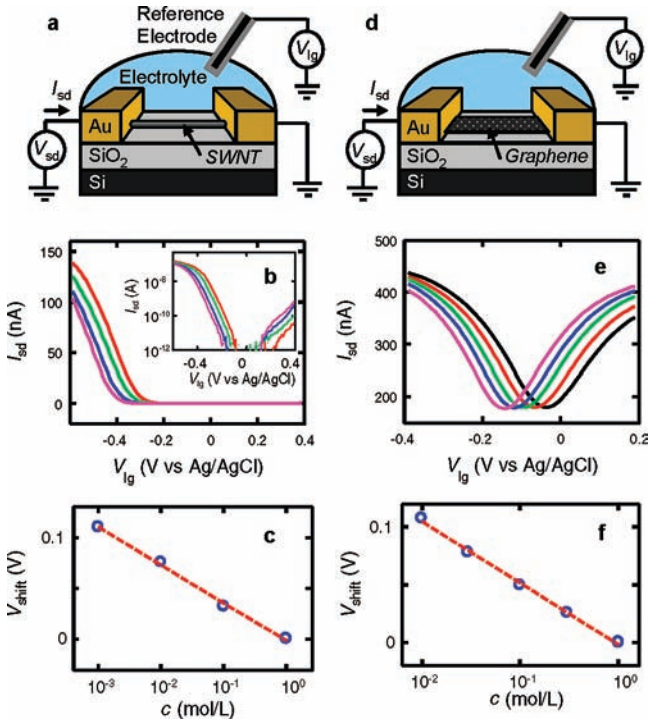

Figure 1. Device layout of SWNT and graphene transistors and corresponding data for electrolyte gating at different salt concentrations. Parts (a) and (d) schematically illustrate device layouts for SWNT and graphene transistors. SWNTs and graphene flakes are electrically contacted with Cr/Au electrodes. A small bias potential, V_{sd}, is applied across the source and drain electrodes, and the source-drain current I_{sd} is monitored. For SWNT devices, we use $V_{sd} = 10$ mV, while for graphene we use $V_{sd} \leq 5$ mV. A liquid-gate potential, V_{lg}, is applied to the electrolyte through an Ag/AgCl reference electrode. The devices are contained in a home-built flow cell for fluidic control (not depicted). (b) $I_{sd}-V_{lg}$ curves measured for a SWNT device in 0.1 mM PB buffer at pH 7 with 1 mM (red), 10 mM (green), 100 mM (blue), and 1 M (magenta) added KCl. The inset shows the same curves on a logarithmic scale. (c) Shift of the $I_{sd}-V_{lg}$ curves in (b), V_{shift}, with respect to the curve measured at 1 M KCl, as a function of the added KCl concentration, c. (e) $I_{sd}-V_{lg}$ curves measured for a graphene device in 1 mM PB buffer at pH 7 with 10 mM (black), 30 mM (red), 100 mM (green), 300 mM (blue), and 1 M (magenta) KCl. (f) Shift of the $I_{sd}-V_{lg}$ curves in (e), V_{shift} with respect to the curve measured at 1 M KCl, as a function of the KCl concentration. The red dashed lines in (c) and (f) are linear fits of V_{shift} versus $\log(c)$.

were buffered using phosphate buffers to control pH. A supporting salt was always present in at least a 10-fold excess of the buffer concentration. We applied a liquid-gate potential, V_{lg}, to the electrolyte via an Ag/AgCl (3 M NaCl) reference electrode.[10] This study presents data for 18 SWNT devices and 13 graphene devices.

Electrolyte Gating of SWNT and Graphene Transistors

We first qualitatively compare electrolyte gating of SWNTs and graphene in aqueous solution. Graphene and SWNTs both consist of sp^2-bonded carbon. Nevertheless, differences in their atomic structure give rise to essential differences in electronic structure: Whereas semiconducting SWNTs exhibit a diameter-dependent band gap of ~0.5 eV, graphene is a zero band gap semiconductor.

Semiconducting SWNTs generally function as Schottky-barrier transistors, in which the gate influences the conductance primarily by changing the Schottky barriers at the interfaces between the SWNT and the source and drain contacts.[11,12] In an electrolyte-gated configuration, the electrolyte gate approaches a near-ideal gate coupling, which allows large Fermi-level shifts,[9,13,14] such that both hole (p) and electron (n) conductance regimes are accessible.[8,15] Figure 1b shows $I_{sd}-V_{lg}$ curves for an individual semiconducting SWNT device in solutions of different KCl concentration buffered at pH 7. At large negative V_{lg}, we observe p-type conductance. Plotted on a logarithmic scale (inset Figure 1b), we see that, after an exponential decrease of p-type conductance with increasing V_{lg} in the subthreshold regime, the current increases again when the SWNT becomes n-doped at positive V_{lg}. Near the potential of minimum conductance, the Fermi level is in the center of the band gap, where there is exactly one occupied π-orbital per carbon atom.

In graphene, conduction is mostly limited by diffusive transport in the channel rather than by Schottky barriers at the contacts. The gate affects the conductance primarily by changing the number of charge carriers and their mobility. Figure 1d shows $I_{sd}-V_{lg}$ curves measured with a graphene transistor at different KCl concentrations at pH 7. The minimum of conductance corresponds to a minimum in the number of charge carriers and occurs near the neutrality point. To the right and left of the neutrality point the majority carriers are electrons and holes, respectively.[16] The magnitudes of the observed Fermi-level shifts are comparable in graphene and in SWNTs.[13,17]

Influence of the Ionic Strength and pH of the Electrolyte

As can be directly seen by inspection of Figure 1b and e, the main consequence of changing the ionic strength is to shift the $I_{sd}-V_{lg}$ curve along the V_{lg}-axis. This indicates that an electrostatic gating effect occurs, whereby the devices become more p-doped with decreasing ionic strength, in agreement with previous studies.[18,19] In Figure 1c and f, we quantify this electrostatic gating effect by plotting the relative shift of the minimum-conductance point, V_{shift}, as a function of salt con-

(10) Minot, E. D.; Janssens, A. M.; Heller, I.; Heering, H. A.; Dekker, C.; Lemay, S. G. *Appl. Phys. Lett.* **2007**, *91*, 093507.

(11) Heinze, S.; Tersoff, J.; Martel, R.; Derycke, V.; Appenzeller, J.; Avouris, P. *Phys. Rev. Lett.* **2002**, *89*, 106801.

(12) Chen, Z.; Appenzeller, J.; Knoch, J.; Lin, Y.; Avouris, P. *Nano Lett.* **2005**, *5*, 1497–1502.

(13) Heller, I.; Kong, J.; Williams, K. A.; Dekker, C.; Lemay, S. G. *J. Am. Chem. Soc.* **2006**, *128*, 7353–7359.

(14) Tarábek, J.; Kavan, L.; Dunsch, L.; Kalbac, M. *J. Phys. Chem. C* **2008**, *112*, 13856–13861.

(15) Männik, J.; Heller, I.; Janssens, A. M.; Lemay, S. G.; Dekker, C. *Nano Lett.* **2008**, *8*, 685–688.

(16) An interesting observation for electrolyte gating graphene is that, in contrast with SWNTs, considerable hysteresis is observed in the $I_{sd}-V_{lg}$ curves, comparable to the situation for back-gating in ambient atmosphere. This is likely related to charges or dipoles trapped underneath the graphene, either in the bulk or on the surface of the oxide. These trapped charges can affect transport in graphene, because for electrolyte-gated graphene, we find that the back-gate coupling is sufficiently strong to affect device conductance, whereas for electrolyte-gated SWNTs, the effect of the back-gate and thus the effect of trapped charges are negligible due to screening of the electric field by the electrolyte that almost entirely encompasses the SWNT. See also ref 24.

(17) The band gap in SWNTs is diameter dependent. Therefore, as the SWNT diameter becomes larger, there is a smooth transition in the $I_{sd}-V_{lg}$ curve shape from semiconducting (Figure 1b) to graphene-like (Figure 1d).

(18) Artyukhin, A. B.; Stadermann, M.; Friddle, R. W.; Stroeve, P.; Bakajin, O.; Noy, A. *Nano Lett.* **2006**, *6*, 2080–2085.

(19) Chen, F.; Qing, Q.; Xia, J. L.; Li, J. H.; Tao, N. J. *J. Am. Chem. Soc.* **2009**, *131*, 9908.

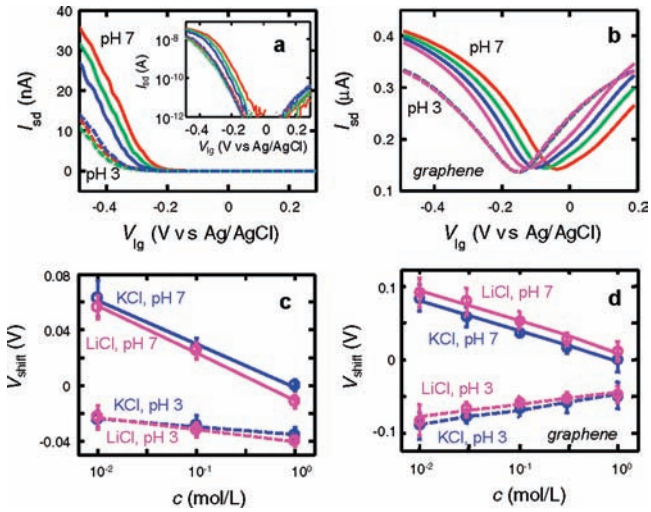

Figure 2. Experimental observations of the electrostatic gating effect for SWNT and graphene devices upon changes in electrolyte concentration, composition, and pH. Parts (a) and (b) show the $I_{sd}-V_{lg}$ curves for a SWNT and a graphene device, respectively, measured in 1 mM PB buffer at pH 7 (solid lines) and pH 3 (dashed lines). In (a), the red, green, and blue curves were measured at 10 mM, 100 mM, and 1 M KCl, respectively. The inset in (a) shows the curves for the SWNT device on a logarithmic scale. In (b), the red, green, blue, and magenta curves were measured at 30 mM, 100 mM, 300 mM, and 1 mM KCl, respectively. Parts (c) and (d) plot the shift, V_{shift}, of the $I_{sd}-V_{lg}$ curves for KCl (blue) and LiCl (magenta), with respect to the $I_{sd}-V_{lg}$ curve measured at 1 M KCl, pH 7. The lines are linear fits of V_{shift} versus log(c) for pH 7 (solid) and pH 3 (dashed). The data in (c) are averaged over 7 SWNT devices, and the data in (d) are averaged over 13 graphene devices.

centration with respect to its value at 1 M KCl.[20] Interestingly, within scatter, V_{shift} depends linearly on log([KCl]) over the 3 orders of magnitude change in concentration covered by our experiments.

To obtain a more complete picture of how electrolyte properties govern electrostatic gating in SWNT and graphene devices, we studied the combined effects of ionic strength, ion type, and pH. Figure 2a and b shows SWNT and graphene transport characteristics in KCl solutions of different ionic strengths at two values of pH. A decrease in pH from pH 7 (solid lines) to pH 3 (dashed lines) causes a shift toward more negative V_{lg}, as previously observed.[21−23] We repeated the experiments using LiCl instead of KCl ($I_{sd}-V_{lg}$ curves not shown), for which we observed qualitatively the same effects when changing pH and ionic strength. Figure 2c and d summarizes these observations by showing the shift of the minimum conductance point as a function of salt concentration averaged over 7 SWNT devices and 13 graphene devices, respectively. The blue lines are linear fits of V_{shift} versus log([KCl]) at pH 7 (solid blue line) and at pH 3 (dashed blue line), while the magenta solid and dashed lines are fits of V_{shift} versus log([LiCl]) at pH 7 and pH 3, respectively. Two important differences between the electrostatic gating effects for SWNTs and graphene are observed. First, the electrostatic gating effect at high pH is larger for graphene than for SWNTs (−32.7 mV/decade averaged over the two salts for SWNTs versus −42.7 mV/decade for graphene). Second, at pH 3 the electrostatic gating effect is qualitatively different for the two types of nanocarbon. For SWNTs, the shift decreases to only −7.3 mV/decade, while for graphene it changes sign to +18.9 mV/decade.

Discussion of the Electrostatic Gating Effect

The observed electrostatic gating effect upon a change in ionic strength is consistent with the presence of a negative surface charge near, but external to the SWNT, as was previously described by Arthyukhin et al.[18] and Back et al.[21] This negative surface charge attracts mobile positive charges to the SWNT−liquid interface, which make the total interfacial charge neutral. These positive charges consist of both positive ions in the electrical double layer in solution and of positive charges (holes) in the SWNT or graphene. What fraction of the negative surface charge is screened by ions in the electrical double layer, and what fraction is screened by charges in the SWNT or graphene, depends on the relative capacitances of these separate components. Typically, the capacitance of the electrical double layer exceeds the intrinisic chemical capacitance, or quantum capacitance, of the nanotube or graphene.[9,24] As a result, most of the negative surface charge is screened by ions in solution. Nevertheless, any extra positive charge in the graphene or SWNT p-dopes the material, which causes the $I_{sd}-V_{lg}$ curve to shift toward more positive gate voltages. The ionic strength and pH effects are best understood in terms of the surface potential at the interface, which gates the transistor. More precisely, the liquid-gate potential experienced by the SWNT or graphene is offset by the potential drop over the electrical double layer in solution that is associated with the negative surface charge. At higher ionic strength, the electrical double layer compresses (i.e., the Debye screening length shortens), which increases the double layer capacitance and reduces the surface potential for a given surface charge. The result of increasing the ionic strength is that the positive shift of the $I_{sd}-V_{lg}$ curve becomes smaller, which will thus shift the curve back to more negative gate potentials as we observed. At low pH, we observed that the curves shift to even more negative V_{lg}. This indicates that the negative charge in the vicinity of the SWNT is pH dependent and is largely neutralized at lower pH. Because of the lower surface charge at low pH, the surface potential is smaller, and thus the ionic-strength-dependent electrostatic gating effect is smaller at low pH. For graphene, we observe that the electrostatic gating at low pH even inverses sign, which indicates that the surface charge even appears positive. This is likely related to the complex surface chemistry of oxidized silicon, for which ionized silanol and silylamine groups can yield both a negatively charged (due to SiO^-) and a positively charged (due to $SiOH_2^+$ and $SiNH_3^+$) surface.

Although previously the negative charge was ascribed to deprotonated silanol groups on the SiO_2 substrate,[18] Back et al.[21] presented a pH-dependent study of suspended SWNTs that provides strong evidence that a significant amount of ionizable groups is also present on the SWNT sidewall.[25,26] Given the high conductivity of both graphene and SWNT transistors, it is unlikely that the ionizable groups on the carbon surface can be

(20) Because for large band gap devices the potential of minimum conductance is poorly measurable due to low current levels in the band gap, a threshold p-conductance value just above the noise level is used instead to define relative shifts of the potential of minimum conductance.

(21) Back, J. H.; Shim, M. *J. Phys. Chem. B* **2006**, *110*, 23736–23741.
(22) Ang, P. K.; Chen, W.; Wee, A. T. W.; Loh, K. P. *J. Am. Chem. Soc.* **2008**, *130*, 14392–14393.
(23) Ohno, Y.; Maehashi, K.; Yamashiro, Y.; Matsumoto, K. *Nano Lett.* **2009**, *9*, 3318–3322.
(24) Heller, I.; Chatoor, S.; Männik, J.; Zevenbergen, M. A. G.; Dekker, C.; Lemay, S. G. *Phys. Status Solidi RRL* **2009**, *3*, 190.
(25) We have observed similar electrostatic gating effects as a function of ionic strength for suspended SWNT transistors (cf., Figure 4).

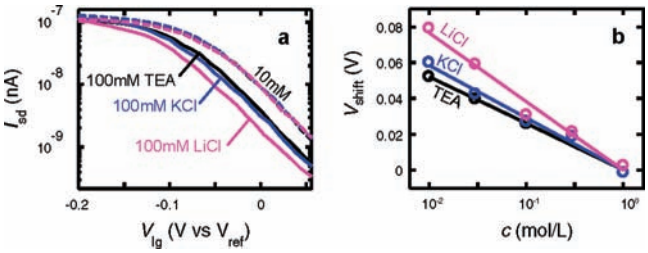

Figure 3. Experimentally observed differences in electrostatic gating of a SWNT device for different types of ions. (a) $I_{sd}-V_{lg}$ curves measured for a SWNT device in 1 mM PB buffer at pH 7. Dashed curves are measured at $c = 10$ mM, and solid curves at $c = 100$ mM, where black, blue, and magenta curves represent tetraethylammonium (TEA) chloride, KCl, and LiCl, respectively. To illustrate the differences in electrostatic gating effect for the different ions, the curves are plotted with respect to V_{ref}, which is taken as the potential for which I_{sd}, measured at $c = 10$ mM for the respective salt, equals 10^{-8} A. (b) The shift, V_{shift}, of the $I_{sd}-V_{lg}$ curves for TEACl (black), KCl (blue), and LiCl (magenta), as a function of c, where the solid lines are linear fits of V_{shift} versus log(c). The data and fits are plotted with respect to the fitted value of V_{shift} at $c = 1$ M for each type of salt.

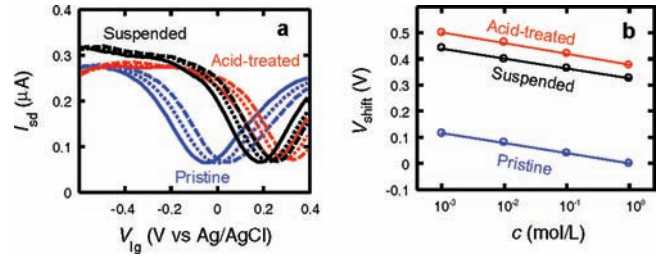

Figure 4. Experimental observation of electrostatic gating effect at different salt concentrations for SWNT devices in pristine (as fabricated) state, after acid treatment, and after suspension. (a) $I_{sd}-V_{lg}$ curves measured for a SWNT device in 1 mM PB buffer at pH 7. Dashed, dotted, and solid curves are measured at 10 mM, 100 mM, and 1 M KCl, respectively. The blue curves are measured in the pristine state, red curves are measured after 20 s fuming nitric acid treatment, and the black curves are measured after suspending the SWNTs above the substrate by underetching the SiO_2 for ~150 nm in buffered HF. (b) The gate-voltage shift of the $I_{sd}-V_{lg}$ curves, V_{shift}, as averaged over 10 devices in pristine state (blue), 10 devices in acid-treated state (red), and 8 devices in suspended state (black). The solid lines are fits of V_{shift} versus log(c). V_{shift} is plotted versus V_{shift} at $c = 1$ M in pristine state.

related to acidic moieties at defect sites in the sp^2 lattice that disrupt the π-conjugated electron system,[28] but rather to acidic functionalities of adsorbents such as resist residues or amorphous carbon (see the Supporting Information for a characterization of possible resist residues).[29,30]

Effect of Different Cations on Electrostatic Gating

Our data in Figure 2 show that the magnitude of the observed electrostatic gating effect depends on ionic strength and pH. In addition, the species of cation appears to quantitatively affect the electrostatic gating effect. The microscopic origin of the apparent ion specificity of the electrostatic gating effect remains unclear. Figure 3 shows experiments with a SWNT device comparing the electrostatic gating effects of LiCl, KCl, and tetraethylammonium chloride (TEA chloride). As opposed to the small alkali cations Li^+ and K^+, TEA^+ is a larger cation that exposes its alkane groups to solution while maintaining high solubility (~300 mM) in aqueous solution. Figure 3a shows the shift of the $I_{sd}-V_{lg}$ curves from 10 mM salt (dashed lines) to 100 mM salt (solid lines), and Figure 3b plots V_{shift} as a function of salt concentration for the three ions. Li^+ (magenta) clearly shows the largest electrostatic gating effect, followed by K^+ (blue), and finally TEA^+ (black). In the Supporting Information, we present two possible explanations for the apparent ion-specific electrostatic gating effect. The first mechanism considers specific cationic adsorption, while the second considers the difference in ionic radii. The latter displaces the plane of closest approach of the ions and thus changes the potential difference between this plane and the transistor surface. Interestingly, graphene exhibits a different apparent ion specific effect than SWNTs (cf., Figure 2c and d). Both mechanisms are consistent with the observations, and more research will be required to assess their relative contributions.

Effect of Surface Preparation on Electrostatic Gating

Figure 4a shows $I_{sd}-V_{lg}$ curves recorded at different KCl concentration for a SWNT-device in three different preparation states.[31] The blue curves show the device in an as-fabricated state, that is, after CVD synthesis and lithography.[29,30] The red curves were recorded on the same device after exposure to HNO_3 for 20 s. Although HNO_3-exposure may induce sidewall defects, the similarity in $I_{sd}-V_{lg}$ curve shapes before and after HNO_3-exposure leads us to conclude that no significant amount of additional sidewall-defects has been introduced. The black curves were obtained after underetching the SiO_2-substrate by ~150 nm using buffered HF. The measurements performed in each preparation state show the familiar electrostatic gating shift as a function of ionic strength. Figure 4b plots V_{shift} as a function of salt concentration in these three preparation states averaged over the 10 SWNT devices, all of which show the same behavior. The average electrostatic gating effect for as-fabricated devices is −39 mV/decade (Figure 4b, blue line), consistent with Figures 1 and 2. After the HNO_3-treatment, the potential of minimum conductance displays a very large shift, on average +377 mV, toward positive V_{lg}. Because the SWNT is neutral at the potential of minimum conductance, the shift of 377 mV can be entirely attributed to a change in electrostatic potential due to a change in the charge density near, but external to, the SWNT. Using a rough estimate of ~7 fF/μm for the electrostatic capacitance of the electrical double layer along the SWNT,[9,13] the corresponding change of external charge is approximately 16 electron charges per nm of SWNT, or about 1 electron charge per 15 carbon atoms. The additional negative charge may originate from a combination of an increased number of ionized silanol groups on the substrate, acidic groups that are created on resist or amorphous carbon residues, and adsorbed chemical species from the HNO_3-treatment (NO_3^-, NO), as was recently

(26) In the case of graphene transistors, the SiO_2 is covered by a single layer of graphene. Because the graphene is impermeable to even monatomic He-gas,[27] it is not at all obvious how the underlying silanol groups are ionized, which also substantiates the possibility of ionizable groups on graphene itself.

(27) Bunch, J. S.; Verbridge, S. S.; Alden, J. S.; van der Zande, A. M.; Parpia, J. M.; Craighead, H. G.; McEuen, P. L. *Nano Lett.* **2008**, *8*, 2458–2462.
(28) Lee, Y. S.; Nardelli, M. B.; Marzani, N. *Phys. Rev. Lett.* **2005**, *95*, 076804.
(29) Heller, I.; Kong, J.; Heering, H. A.; Williams, K. A.; Lemay, S. G.; Dekker, C. *Nano Lett.* **2005**, *5*, 137–142.
(30) Ishigami, M.; Chen, J. H.; Cullen, W. G.; Fuhrer, M. S.; Williams, E. D. *Nano Lett.* **2007**, *7*, 1643–1648.

(31) This particular SWNT has a very small band gap such that the electronic transport properties display strong similarities to those of graphene (cf. Figure 1e).

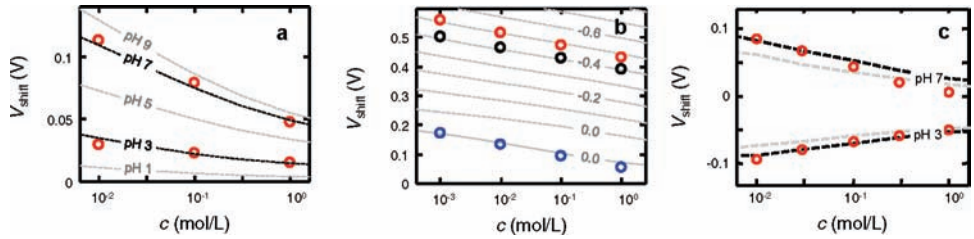

Figure 5. Comparison of experimentally observed electrostatic gating effect (○) with modeling (lines). Part (a) compares V_{shift} as a function of salt concentration, c, for SWNTs, as previously presented in Figure 2c. The data for LiCl and KCl have been averaged (red ○). Dashed lines represent the surface potential ψ_S, calculated using the model and parameters explained in the text, using different values of the pH as indicated in the graph. (b) V_{shift} as a function of salt concentration at pH 7 for SWNT devices in pristine (blue), acid-treated (red), and suspended (black) state, as previously presented in Figure 4b. Gray lines represent the surface potential ψ_S, calculated using the model and parameters explained in the text, using different values of σ_{offset}, as indicated in the graph in C/m^2. Solid and dashed lines use $\sigma_{max} = 0.75$ e/nm^2 and $\sigma_{max} = 2$ e/nm^2, respectively. (c) V_{shift} as a function of salt concentration for graphene devices, as previously presented in Figure 2d. The data for LiCl and KCl have been averaged (red ○). Dashed lines represent the surface potential ψ_S, calculated in cylindrical (gray) and planar (black) geometry, respectively, at pH = 3 and pH = 7, as indicated in the graph.

demonstrated.[32] Strikingly, although the charge surrounding the SWNT appears to have increased dramatically, the average electrostatic gating effect as a function of salt concentration remains relatively unchanged (−42 mV/decade, Figure 4b, red line) as compared to the as-fabricated state. In the suspended state, ionized silanol groups from the SiO_2 substrate are at a distance of at least ∼150 nm from the SWNT and can thus no longer significantly contribute to electrostatic gating of the SWNT. The $I_{sd}-V_{lg}$ curves shift partially back toward negative V_{lg} by 53 mV on average. The electrostatic gating effect as a function of salt concentration in the suspended state (−38 mV/decade, Figure 4b, black line) is, however, again comparable to the electrostatic gating effect in the previous two states. The striking conclusion from the data in Figure 4 is that the absolute charge density near the SWNT, over the range of charge densities probed in this experiment, appears to have a minor effect on the magnitude of the electrostatic gating effect as a function of salt concentration. Furthermore, the electrostatic gating effect observed in the suspended state indicates the presence of negatively charged groups on the SWNT surface.

Model of the Electrostatic Gating Effect

We now derive a model of the surface potential as a function of electrolyte and surface properties that can explain the majority of the observed electrostatic gating effects. The surface potential at the outer Helmholtz plane, ψ_{OHP}, which is the plane of closest approach of solvated ions at a distance x_{OHP} away from the surface, is related to the charge of ionized surface groups that are in equilibrium with protons in solution.[33] We take into account that a distribution of proton association energies may occur at these unknown ionizable surface groups by using a Langmuir−Freundlich adsorption isotherm.[21] In addition to the pH-dependent surface charges, an extra contribution to the surface charge density, σ_{offset}, may arise from ionized groups that are relatively independent of the surface proton concentration in the probed range. We can write for the total surface charge due to ionized surface groups:

$$\sigma_{IG}(\psi_{OHP}) = \frac{\sigma_{max}}{1 + 10^{m(pK_a - pH)} \exp(-m\beta e\psi_{OHP})} + \sigma_{offset} \quad (1)$$

where σ_{max} is the surface charge at 100% dissociation, m reflects the degree of heterogeneity between binding sites, e is the electron charge, $\beta = 1/kT$, k is the Boltzmann constant, T is temperature, ψ_{OHP} is the electrostatic potential at the outer Helmholtz plane, and pK_a is the average acid dissociation constant for the pH-dependent ionizable groups. We determine the surface potential induced by this surface charge using the Poisson−Boltzmann equation. For a planar geometry (i.e., graphene), this relation is given in the form of the Grahame equation:[34]

$$\sigma_{PB}(\psi_{OHP}) = \frac{\varepsilon_r\varepsilon_0\kappa}{\beta e} \sinh\left(\frac{\beta e\psi_{OHP}}{2}\right) \quad (2)$$

Here, the subscript PB indicates that $\sigma_{PB}(\psi_{OHP})$ satisfies the Poisson−Boltzmann equation, ε_r and ε_0 are relative and vacuum permittivity, κ^{-1} is the Debye screening length $\kappa^2 = 2\beta e^2 n/\varepsilon_r\varepsilon_0$, and n is the concentration of monovalent salt.[34] For SWNTs, we use the approximate solution to the Poisson−Boltzmann equation in cylindrical coordinates as given by Ohshima.[35,36] We self-consistently solve $\sigma_{PB}(\psi_{OHP}) = \sigma_{IG}(\psi_{OHP})$, which yields the potential at $x = x_{OHP}$, ψ_{OHP}. To calculate the surface potential, ψ_S, at $x = 0$, we also take into account the change in potential from $x = x_{OHP}$ to $x = 0$. Assuming no charge closer than x_{OHP}, the Poisson equation, $\nabla^2\psi = 0$, implies that $\psi(x)$ changes linearly with distance in the planar case and logarithmically in the cylindrical case (in the latter case, x is offset by the nanotube radius, which we assume to be 1 nm). Consequently, we can combine Gauss' law, $\sigma = -\varepsilon_r\varepsilon_0(\delta\psi/\delta x)_{xOHP}$ with equation 2 to give, for the planar case, $\psi_S = \psi_{OHP} + (\kappa x_{OHP}/\beta e)\sinh(\beta e\psi_{OHP}/2)$, which we directly compare to V_{shift}. For the cylindrical case, we use the corresponding $\sigma_{PB}(\psi)$ relation given by Ohshima.[35]

Figure 5 compares the salt-concentration-dependent V_{shift} data that we presented previously in Figures 2 and 4 (open symbols) to the above-mentioned model (curves). We use $x_{OHP} = 4$ Å and $\varepsilon_r = 80$. Because of the strong evidence that a considerable part of the electrostatic gating is due to acidic groups on organic adsorbents, we use the pK_a of carboxylate moieties ($pK_a \approx 4.5$). Figure 5a shows V_{shift} as a function of salt concentration as presented previously in Figure 2b for SWNTs. The surface potential versus salt concentration curves are based on a

(32) Chou, A.; Bocking, T.; Liu, R.; Singh, N. K.; Moran, G.; Gooding, J. J. *J. Phys. Chem. C* **2008**, *112*, 14131–14138.
(33) Behrens, S. H.; Grier, D. G. *J. Chem. Phys.* **2001**, *115*, 6716–6721.
(34) Bard, A. J.; Faulkner, L. R. *Electrochemical Methods, Fundamentals and Applications*, 2nd ed.; John Wiley & Sons: New York, 2001.
(35) Ohshima, H. *J. Colloid Interface Sci.* **1998**, *200*, 291–297.
(36) The approximate solution of ref 35 assumes an infinite cylinder, which is a reasonable assumption for a nanotube with an aspect ratio ∼1000. The approximated surface potential−surface charge relation exhibits an error of typically 1% as compared to numerical solutions over the experimentally explored range (ionic strength ∼1 mM to 1 M and $\psi_{OHP} < 4k_BT$). The largest error (6.6%) occurs for low ionic strength (1 mM) and high ψ_{OHP} ($4k_BT$).

cylindrical geometry and use $\sigma_{max} = 0.5$ e/nm^2, $m = 1/3$ (similar to ref 21), and values for the pH as indicated in the graph. As is obvious from Figure 5a, the model describes the data quite well. From this comparison, we conclude that it is very plausible that the V_{shift} arises from the surface potential induced by ionizable surface groups, which are present at densities of the order of ~1 per nm^2. From our data, it is not possible to determine the exact pK_a of these surface groups. We can, however, conclude that a reasonable fraction of the surface groups should have a pK_a near 4.5 or lower to maintain a finite electrostatic gating effect of several millivolts per decade at pH 3.

In Figure 5b, we compare to the model the data of Figure 4, where the electrostatic gating effect of SWNTs in as-fabricated, acid-treated, and suspended state was presented. The gray solid line, for which we used $\sigma_{max} = 0.75$ e/nm^2, describes the data in the as-fabricated state reasonably well. The acid treatment is expected to increase the number of acidic moieties due to oxidation, which was taken into account by modeling an increase in σ_{max} to 2 e/nm^2. Furthermore, we observed a large shift in the potential of minimum conductance, which we concluded to be related to a large increase in negative charge near the SWNT. It was recently shown that nitric acid treatment of SWNTs causes significant adsorption of NO_3^- ions.[32] Because NO_3^- has a pK near -2, it is relatively pH independent under the experimentally probed conditions. In our model, this is taken into account by setting $\sigma_{offset} < 0$. The gray dashed lines in Figure 5b are calculated using $\sigma_{max} = 2$ e/nm^2, and σ_{offset} ranging from 0 to -0.8 C/m^2, as indicated in the graph. The data for acid-treated and suspended SWNTs are consistent with the model for values of σ_{offset} of, respectively, -0.5 and -0.4 C/m^2. Importantly, the model reproduces well the observation that the electrostatic gating effect as a function of salt concentration is relatively independent of the total surface charge.

Finally, in Figure 5c we compare the electrostatic gating data for graphene to our model. The black dashed lines indicate the pH 3 and pH 7 curves for graphene, which were calculated using $m = 1/2$, and assuming a planar geometry. To accommodate the sign inversion between the two pH values, the model assumes the presence of two types of ionizable groups, one of which is protonated from a -1 e charge to a neutral charge, and another type that is protonated from a neutral charge to a $+1$ e charge. The maximum surface charge of both types of ionizable groups is taken as $\sigma_{max} = \pm 0.5$ e/nm^2. For simplicity, we assume a pK of 4.5 for both types of ionizable groups. The planar model with two types of ionizable groups matches the data quite well, except for the high pH, high ionic strength regime. The gray dashed lines use the exact same set of parameters used to define the black lines, but calculated using a cylindrical geometry instead of a planar geometry. The planar case yields a larger electrostatic gating effect than the cylindrical case, which is in agreement with the larger experimentally observed electrostatic gating effect for graphene than for SWNTs (cf., Figure 2c and d). In the model, the increased electrostatic gating effect is due to the less efficient screening of local electric fields in a planar geometry, which leads to higher surface potentials.

The comparison of our electrostatic gating data to modeling of the surface potential as a function of the electrolyte composition shows that the majority of the data can be explained by the presence of ionizable groups external to the SWNT or graphene. The qualitative pH dependence and ionic-strength dependence are well reproduced. In addition, the models confirm that a larger electrostatic gating effect is expected for graphene than for SWNTs. The exact chemical identity of the ionizable groups, however, cannot be directly deduced from these experiments. Finally, our model ignores ion-specific effects, which can provide a better agreement between model and data and further explain the detailed response of the transistors to changes in electrolyte composition (see the Supporting Information). Additional mechanisms might also play a role, such as a decrease of dielectric constant in the double layer.[37]

Effect of Ionic Strength on p-type and n-type Conductance

Up to this point, we have only considered the electrostatic gating effect upon changing ionic strength and pH. Other possible interaction mechanisms of nanoscale transistors with aqueous solutions include Schottky-barrier modulation, changes in gate capacitance, and changes in carrier mobility.[8] These three mechanisms primarily affect the shape of the $I_{sd}-V_{lg}$ curves. The remainder of this Article will focus on changes in $I_{sd}-V_{lg}$ curve shape for SWNTs. An equivalent analysis could not be carried out for graphene because of the significant hysteresis in the $I_{sd}-V_{lg}$ curves.[16]

Figure 6a shows $I_{sd}-V_{lg}$ curves for a small band gap SWNT at 1 M (solid line) and 1 mM KCl (dashed line) at pH 7. The curves are plotted with respect to the potential of minimum conductance to correct for electrostatic gating effects. Interestingly, we observe both a p-type and an n-type conductance decrease with decreasing ionic strength. In Figure 6b, we quantify this effect by plotting the relative conductance change with respect to 1 M salt, $\Delta G/G_{1M}$, as a function of salt concentration. Linear fits of the $\Delta G/G_{1M}$ data versus log(c) yield $\Delta G_P = -0.9\%$ per decade decrease of [KCl] for hole conductance (black line) and $\Delta G_N = -1.4\%$ per decade decrease of [KCl] for electron conductance (gray line). In Figure 6c, we show a scatter plot of ΔG_N versus ΔG_P, where the "○" represent 10 SWNT devices. (The inset shows two additional outlying data points.) Interestingly, 9 out of 10 SWNT devices are located in the hatched quadrant that indicates both negative ΔG_P and ΔG_N. This is a clear indication that the mechanism responsible for these conductance changes is either a change in gate capacitance or a change in carrier mobility.[8] We can, however, disregard the carrier mobility effect: Because for micrometer-long semiconducting SWNT transistors the conductance is in general limited by the Schottky-barriers at the contacts,[11,12] the intrinsically high carrier mobility[38] is expected to have a negligible effect on device conductance.[8] In contrast, for small band gap SWNTs, the carrier mobility plays a dominant role. Therefore, if the observed conductance changes are related to carrier mobility changes, we expect to observe much larger conductance changes for small band gap SWNTs than large band gap SWNTs. Because we do not observe this experimentally, we rule out the carrier-mobility effect. We therefore conclude that the symmetric conductance decrease with decreasing ionic strength is most likely related to an ionic-strength-dependent change in gate capacitance.

Modeling the Gate Capacitance Effect as a Function of Ionic Strength

We can estimate the gate capacitance effect of a change in salt concentration on the shape of the $I_{sd}-V_{lg}$ curve. The total

(37) Kolb, D. M. *Angew. Chem., Int. Ed.* **2001**, *40*, 1162–1181.
(38) Dürkop, T.; Getty, S. A.; Cobas, E.; Fuhrer, M. S. *Nano Lett.* **2004**, *4*, 35–39.

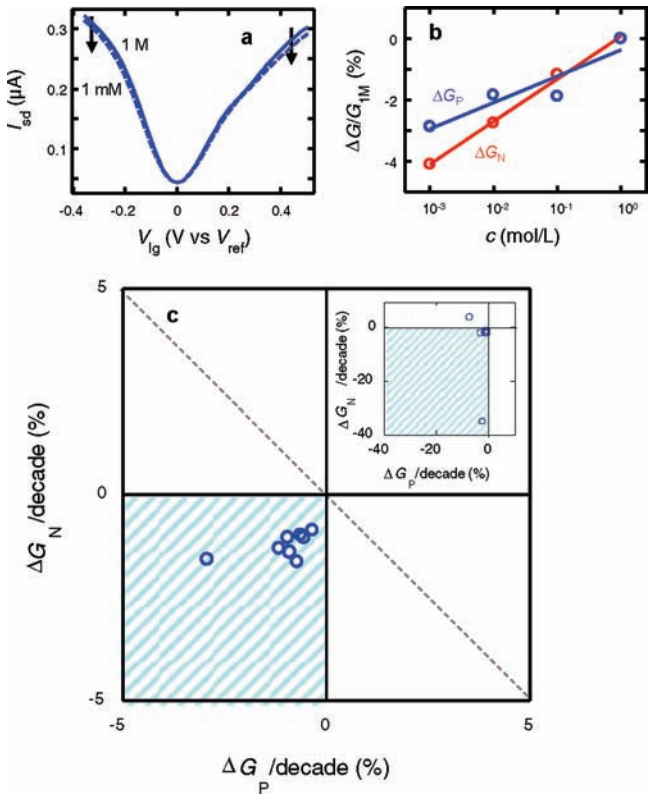

Figure 6. Analysis of p-type and n-type conductance changes as a function of salt concentration for SWNT devices. (a) $I_{sd}-V_{lg}$ curves, plotted with respect to the potential of minimum conductance, for a small band gap SWNT measured at pH 7, at 1 M KCl (solid line),and at 1 mM KCl (dashed line). (b) Relative change in p-type (blue) and n-type (red) conductance, $\Delta G/G_{1M}$, for the device of (a), as a function of KCl concentration, c, normalized to the conductance measured at 1 M. Here, G is averaged over 50 mV at the extreme ends of the potential range over which the $I_{sd}-V_{lg}$ curves overlap, after correcting for electrostatic gating. The solid lines are linear fits of $\Delta G/G_{1M}$ versus log(c). (c) Scatter plot of ΔG_N versus ΔG_P, obtained from linear fits as in (b) for 10 SWNT devices (○). The inset shows the same data set on a larger scale, revealing two outlying data points. As explained in ref 8, points in the hatched quadrant are indicative of carrier mobility and gate capacitance changes, while points near the gray dashed line, $\Delta G_P = -\Delta G_N$, indicate workfunction modulation.

gate capacitance for a SWNT consists of the intrinsic chemical capacitance of the SWNT, the quantum capacitance C_q, in series with the double-layer capacitance, C_{dl}.[13] Although in general C_q is the smaller of the two and thus dominates the interfacial capacitance, we have previously argued against ignoring the electrostatic potential drop over the double layer, which reduces the gate efficiency and thus the Fermi-level shift.[13] Indeed, recently Tarábek et al. confirmed experimentally that the Fermi-level shift for electrolyte-gated SWNTs at 1 V liquid-gate potential is significantly smaller than 1 eV.[14] To calculate $C_{dl} = d\sigma_{PB}/d\psi_S$, we differentiate the $\sigma_{PB}(\psi_S)$ relations that we previously derived.

The quantum capacitance C_q also depends on the gate potential.[13,24] We model the gate dependence of C_q as described in ref 13. Figure 7a plots the calculated Fermi-level shift as a function of V_{lg}, for two different salt concentrations. Here, we use $\psi_{OHP} = -100$ mV when the SWNT is neutral as a reasonable estimate for the potential at the outer Helmholtz-plane due to a negative surface charge density of 1 e/nm^2. It is clear that a decrease of salt concentration indeed decreases the Fermi-level shift due to reduced gate efficiency. Consequently,

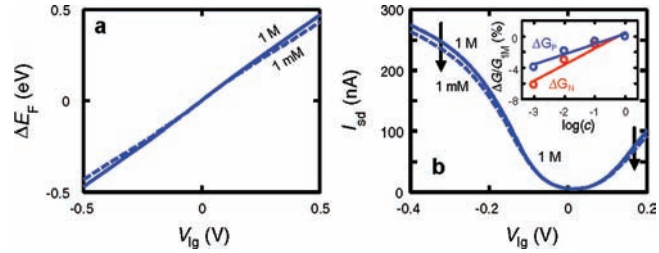

Figure 7. Modeling of the effect of salt-dependent gate capacitance changes on transport properties for SWNTs. Part (a) shows calculations of the Fermi-level shift ΔE_F as a function of V_{lg}, at 1 M KCl (solid line) and 1 mM KCl (dashed line) at pH 7. Part (b) calculates the corresponding change in $I_{sd}-V_{lg}$ curves using the model in ref 8. The inset in (b) shows the relative conductance change, $\Delta G/G_{1M}$, determined as in Figure 6b from the change in conductance averaged over 50 mV at the opposite extreme end points of the calculated potential range. The blue and red lines are linear fits of $\Delta G/G_{1M}$ versus log(c).

the $I_{sd}-V_{lg}$ curve widens, and both p-type and n-type conductance decrease for a fixed V_{lg}.

To illustrate the effect of an ionic-strength-dependent change in gate efficiency, we calculate the change in $I_{sd}-V_{lg}$ curve-shape using a model that describes transport in Schottky-barrier SWNT-transistors as explained previously in ref 8.[39] Figure 7b plots the calculated $I_{sd}-V_{lg}$ curves that correspond to the Fermi-level shifts plotted in Figure 7a. The change in the calculated $I_{sd}-V_{lg}$ curves is in good qualitative agreement with the experimentally observed change in $I_{sd}-V_{lg}$ in Figure 6a. Furthermore, the inset in Figure 7b shows the relative conductance changes as a function of the salt concentration, yielding $\Delta G_P = -1.3\%$ per decade and $\Delta G_N = -2.1\%$ per decade, in good agreement with our data. Although the previous calculation was performed for SWNTs, C_{dl} and C_q for graphene are directly comparable to those for SWNTs,[13] which means that the calculated decrease in gate efficiency should also apply for graphene.[40]

Effect of pH on p-type and n-type Conductance

Finally, we evaluate the effect of pH on the $I_{sd}-V_{lg}$ relation for electrolyte-gated SWNT transistors.[42] Figure 8a shows $I_{sd}-V_{lg}$ curves of a small band gap SWNT at pH 3 and pH 7. As indicated by the arrows in Figure 8a, a decrease in p-type conductance and an increase in n-type conductance, indicative

(39) To calculate the curves in Figure 7b, an exponential band-bending profile with typical length-scale of 1 nm, independent of salt concentration, was used. See ref 8.

(40) Although the decreased gate capacitance provides a satisfying explanation for the observed decrease in p-type and n-type conductance upon decreasing salt concentration, other mechanisms may yield similar effects. When we derived a model for calculating $I_{sd}-V_{lg}$ curves for SWNTs in ref 13, we assumed that the band-bending profile at the contacts is given by the potential drop in the double layer. Thus, if the Debye length is longer at low salt, the Schottky barriers are wider, which would also lead to a decrease in p-type and n-type conductance. We, however, disregard this mechanism, because this Schottky-barrier-width effect is band gap dependent and should largely disappear for graphene, which we do not observe experimentally. We speculate that the reason for the absence of this effect is that, first, most of the electrostatic potential drop at the contact occurs over the thin Stern layer, which is independent of salt concentration. Secondly, the average position at which electrons tunnel from the metal into the SWNT is not likely to be exactly at the point where SWNT, metal, and electrolyte ions meet.[41] If the average entry point lies buried under the metal, the contribution of the potential profile in solution to the average Schottky-barrier width should decrease.

(41) Nakanishi, T.; Bachtold, A.; Dekker, C. *Phys. Rev. B* **2002**, *66*, 073307.
(42) Van den Berg, A.; Bergveld, P.; Reinhoudt, D.; Sudholter, E. *Sens. Actuators* **1985**, *8*, 129.

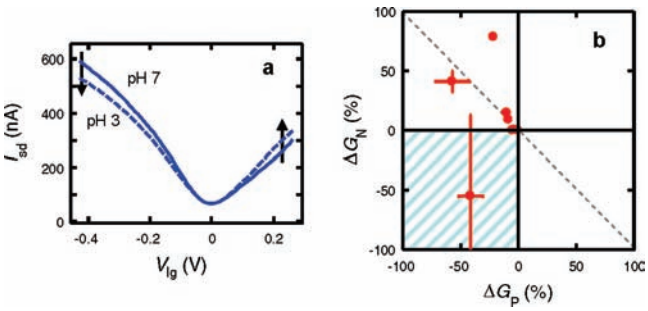

Figure 8. Analysis of p-type and n-type conductance changes as a function of pH for experiments with SWNTs. Part (a) shows $I_{sd}-V_{lg}$ curves, averaged for 1 M, 100 mM, and 10 mM KCl and LiCl at pH = 7 (solid line) and pH = 3 (dashed line). Part (b) shows a scatter plot of ΔG_N versus ΔG_P for 7 SWNT devices, where ΔG is defined as the relative change of conductance when changing from pH 7 to pH 3. We calculate ΔG by averaging the conductance change over 50 mV at the extreme ends of the V_{lg} range after correction for electrostatic gating. This conductance change is averaged over the three different salt concentrations and two different salts and is plotted in (b). The error bars represent the standard deviation of ΔG over the 50 mV range, averaged over the different salt concentrations and different salts.

of the Schottky-barrier mechanism, is observed when the pH is lowered from pH 7 to pH 3. Figure 8b shows a scatter plot of ΔG_N versus ΔG_P for 7 SWNT devices. Interestingly, 6 out of 7 devices exhibit a positive ΔG_N and a negative ΔG_P upon lowering pH.[43] We attribute this Schottky-barrier effect to modulation of the work-function difference between metal and SWNT due to a change in the ionization state of surface groups near the contacts when lowering pH.

Conclusions and Implications

In summary, we have observed an intricate response of the transport characteristics of electrolyte-gated SWNT and graphene transistors to changes in electrolyte properties like pH, salt concentration, and the type of ions present. Our findings have significant implications for (bio)sensing with SWNT and graphene transistors. In sensing experiments, where specificity is often an important issue, changes in the electrical signal can be effected both by charged target (bio)molecules and, as we showed here, by electrolyte ions. Careful and judicious control of electrolyte properties is required to isolate the sensor response to target molecules. The sensor response to either target molecules or changes in electrolyte properties can, however, be diagnosed through examination of changes in ambipolar transport behavior, where the models derived in this report and ref 8 may serve to make rough quantitative estimates of the changes in physical parameters that induce sensor response. Alternatively, the large response of nanosensors to electrolyte properties may be taken advantage of in sensing experiments where processes are monitored that change the electrolyte properties on a local scale. In the context of optimizing the sensitivity of sensing experiments, the importance of the Debye screening length in biosensing experiments has recently been discussed.[44,45] Although it is intuitive that the most sensitive measurements can be performed at low salt concentration, our data show that, in case devices have a high surface charge density, the sensor response to adsorbed charges is relatively independent of the salt concentration (cf., Figure 4b). On the other hand, decreasing the intrinsic surface charge of the sensor can increase its charge sensitivity. We also demonstrated that an analysis of sensor response to changes in electrolyte properties can help to diagnose the presence of ionizable groups, estimate the sign and magnitude of the surface charge density, and test sensitivity to the different sensing mechanisms. With a better understanding of the fundamental electrostatic interactions that affect transport in SWNT and graphene sensors, improvements can be made on optimization and interpretation of sensing experiments with these promising, high sensitivity nanosensors.

Acknowledgment. We thank Ethan D. Minot for helpful discussions. This work was financially supported by NWO and NanoNed.

Supporting Information Available: Device fabrication methods and modeling of ion-specific electrostatic gating. This material is available free of charge via the Internet at http://pubs.acs.org.

JA104850N

(43) Although we have also measured transport in graphene transistors at different pH, we observed a difference in hysteresis at different pH. Consequently, the relative curve shapes cannot be compared.

(44) Stern, E.; Wagner, R.; Sigworth, F. J.; Breaker, R.; Fahmy, T. M.; Reed, M. A. *Nano Lett.* **2007**, *7*, 3405–3409.
(45) Nair, P. R.; Alam, M. A. *Nano Lett.* **2008**, *8*, 1281–1285.